Article

A Numerical Study on the Crack Propagation of Homogenized Micro-Crack Crushing for Concrete Pavement

Wenjie Li [1], Ying Guo [1], Bin Liang [1] and Jinchao Yue [2],*

[1] School of Civil Engineering, Henan University of Science and Technology, Luoyang 471023, China; liwenjie041@126.com (W.L.); gytha_ying@163.com (Y.G.); liangbin4231@163.com (B.L.)
[2] School of Water Conservancy Engineering, Zhengzhou University, Zhengzhou 450001, China
* Correspondence: yuejc@zzu.edu.cn

Abstract: Homogenized micro-crack crushing is a new method of concrete pavement rehabilitation that makes full use of the bearing capacity of the original concrete pavement, whereby the treated pavement can be directly overlaid with hot mixed asphalt concrete. In order to solve the problem of longitudinal crack extension of a cracked core in the weak position of local pavement, the crack propagation mode of concrete slabs under low-velocity impact from different numbers and distributions of impact heads was studied using numerical simulation. Moreover, field tests were also carried out to determine the optimal layout of drop hammer impact heads, and the numerical simulation results were compared with the experimental data. The results show that, when a concrete slab is impacted by a single impact head, the bottom of the slab first cracks and then the crack develops upward until the main crack runs through the concrete slab. However, when the concrete slab is impacted by multiple-impact heads, including three or four impact heads, the concrete slab forms a triangular or quadrilateral fracture core, respectively. The numerical simulation results are in good agreement with the laboratory experiments. Through the optimized arrangement of the hammer's impact heads, the problem of longitudinal crack extension of a cracked core can be effectively solved, and the probability of reflection cracks can be reduced.

Keywords: PCC pavement; homogenized micro-crack impact crushing; numerical simulation; fracture mechanism; hammer optimization

1. Introduction

During the service period of concrete pavement, the bearing capacity of the foundation is easily reduced due to the infiltration of surface water. This leads to the formation of a void at the bottom of the pavement, causing the pavement to become prone to cracking. When the concrete pavement reaches its designed service life, various problems will appear successively on the concrete pavement—mainly including corner break, cracks, depressions, pavement pumping, and faulting of the slab ends—which seriously affect road traffic safety. When routine maintenance cannot guarantee the performance of the pavement, it needs to be rehabilitated, and the pavement should be removed or broken up for reuse. The removal cost is relatively high, and it often has an adverse impact on the environment. Recycling after crushing can not only effectively utilize the original concrete pavement, but also effectively solve the problem of reflection cracks in a "white to black" rehabilitation project [1,2].

Among the old concrete-pavement-crushing and reconstruction methods, homogenized micro-crack crushing is a novel concrete-pavement-crushing technology. This method combines the advantages of multiple head breakers, impact compactors, guillotine breakers, and resonant pavement breakers, which makes full use of the bearing capacity of the original pavement and treats the corresponding problems [3–8]. When old concrete pavement is rehabilitated by homogenized micro-crack crushing technology, special mechanical equipment is used to crush the old concrete pavement. This causes the inside of the

cement pavement slab to form oblique micro-cracks evenly distributed in all directions, and the cracked concrete blocks will be interlocked with each other. This not only effectively overcomes the generation of reflection cracks, but also maximizes the bearing capacity of the original concrete pavement. After the old concrete pavement undergoes homogenized micro-crack crushing, the asphalt pavement can be directly overlaid [9].

The homogenized micro-crack rehabilitation of concrete pavement is carried out along the driving direction of the road. Due to problems such as insufficient base bearing capacity and insufficient strength of the concrete pavement in some of the reconstructed sections, if the two front and back impact rupture areas are closely adjacent or partially overlapping during the crushing process, the cracks between the two areas will become connected to each other along the driving direction, as shown in Figure 1. When the asphalt pavement is overlaid, it is easy to produce longitudinal reflection cracks in the driving direction. The local weak base of the concrete pavement can be reinforced by grouting, but the longitudinal crack extension of the cracked areas still needs to be treated so as to better prevent the occurrence of longitudinal reflection cracks in the asphalt pavement.
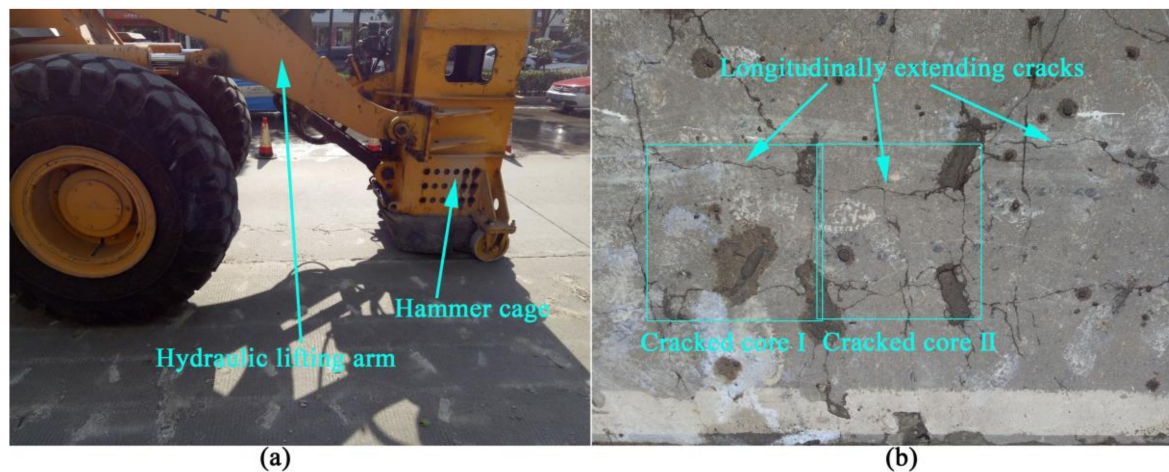

Figure 1. Crack extension of the cracked areas. (**a**) Impact crushing equipment; (**b**) Crack development of cracked core.

In the homogenized micro-crack crushing of concrete pavement, the crack propagation and the fracture state of the concrete slab are the key points that need to be studied. Low-velocity impact fractures from concrete slab testing will be helpful for understanding the homogenized micro-crack crushing fracture mechanism. In terms of the impact resistance of plain concrete and the different types of concrete-based composites, many low-velocity impact tests have been carried out on concrete slabs. Nia, Hedayatian, and Nili et al. [10] conducted impact tests and numerical simulations on plain concrete (PC) and fiber-reinforced concrete (FRC), and found that an increase in the fiber volume fraction greatly increased the impact resistance of the concrete specimens. Sakthivel, Ravichandran, and Alagamurthi [11] developed a hybrid steel mesh-and-fiber-reinforced cementitious composite (HSMFRCC) and studied its impact resistance. They found that the impact resistance of HSMFRCC was higher than SMRCC (steel-mesh-reinforced cementitious composites). Yahaghi, Muda, and Beddu [12] conducted impact tests on oil palm shell lightweight concretes reinforced by polypropylene (PP) fibers, and found that there was a strong linear relationship between the volume fraction of the PP fibers and the impact resistance. Through low-velocity impact tests, Elavarasi and Mohan [13] studied the responses of thin slabs of slurry-infiltrated fibrous concrete (SIFCON) with and without reinforcement, and found that binary blends of silica fume and slag improved the strength and durability characteristics significantly. Othman and Marzouk [14,15] conducted low-velocity impact tests of high-strength concrete (HSC) and ultra-high-performance fiber-reinforced concrete (UHP-FRC) plates to study the impact resistance, and found that the UHP-FRC plates ex-

hibited better damage control characteristics than the high-strength concrete (HSC) plates. Moreover, the crack pattern and failure mode were more dependent on the reinforcement arrangement rather than reinforcement ratio. Xiao, Li, and Fujikake [16] conducted low-velocity impact tests on concrete slabs to study the impact resistance of reinforced concrete slabs, and found that the damage to slabs under a low-velocity impact increased with increasing impact energy. From the test results, it was found that the failure mode of a concrete slab changes with a change in the impact conditions. Yoo and Yoon [17] estimated the impact resistance of steel-fiber-reinforced concrete slabs strengthened with fiber-reinforced polymer sheets, and found that the impact resistance of the steel-fiber-reinforced concrete slabs was substantially improved by externally strengthening the fiber-reinforced polymer sheets. Ganesan and Kumar [18] studied the deflection of prestressed and reinforced concrete (RC) slabs supported with different end conditions, and found that the effectiveness of prestressing on the impact resistance capacity of RC slabs could be demonstrated by comparing the deflection of RC slabs under similar impact loadings. Anil, Kantar, and Yilmaz [19] studied the behavior of RC slabs subjected to impact loading under different support conditions, and finite element analyses using ANSYS Explicit STR software were also conducted to simulate the low-velocity experiments.

In summary, most of the aforementioned studies primarily focused on the impact resistance characteristics of plain concrete, reinforced concrete, fiber-reinforced concrete, and fiber-reinforced concrete-based composites, and they were carried out by considering the aspects of concrete ratio, reinforcement ratio, fiber production ratio, concrete slab support types, and so on. To our best knowledge, little work has been reported that addresses the fracture mechanism of concrete slabs and the propagation mode of micro-cracks under the low-velocity impact of a drop hammer with different impact heads. In this study, through numerical simulation, the fracture mechanism and crack propagation mode of concrete slabs under low-velocity impact were innovatively studied under the conditions of different impact heads and different impact heights. Combined with the results of previous indoor tests, the development law of micro-cracks in concrete slabs was verified by comparison. At the same time, according to the fracture law of concrete slabs in concrete pavement during field tests, the impact device of the fracture equipment was improved and optimized, which effectively avoided the extension and penetration of longitudinal cracks and reduced the probability of the occurrence of reflective cracks in the asphalt pavement.

2. Numerical Simulation

2.1. Numerical Modeling

The numerical model of impact testing included a drop hammer, bearing plate, impact head, and concrete plate. Solid164 solid elements were used for each part, and all were divided by hexahedral meshes. The numerical models of the impact tests under different working conditions are shown in Figure 2, in which the types of drop hammer impact heads included a single impact head, three impact heads, and four impact heads. Among them, there were two working conditions for the four-impact-head tests; one where the long axis of the impact head was along the diagonal direction of the concrete slab (Condition I), and the other where the long axis of the impact head was along the direction of the symmetry axis of the concrete slab (Condition II). Working Condition I was consistent with the actual micro-crack crushing process during the rehabilitation of concrete pavement. For the numerical simulation process of the on-site concrete pavement homogenized micro-crack crushing construction and the indoor concrete slab drop-weight impact tests [9], the main material parameters are shown in Table 1 and the parameters of different impact test conditions are shown in Tables 2 and 3. In the process of modeling and analyzing with LS-DYNA, it was necessary to deal with the collision and contact problems of each part. When defining the contact of each part, the contact surface was defined as a set of quadrilateral and triangular regions, where one surface was defined as the master surface and the corresponding surface was the slave surface. In order to ensure correct contact of

each part of the impact system and no penetration of the node meshes of each part, the falling weight and the bearing plate were defined as automatic face-to-face contact, while the impact head of the bearing plate and the concrete slab were defined as face-to-face erosion contact [20,21].
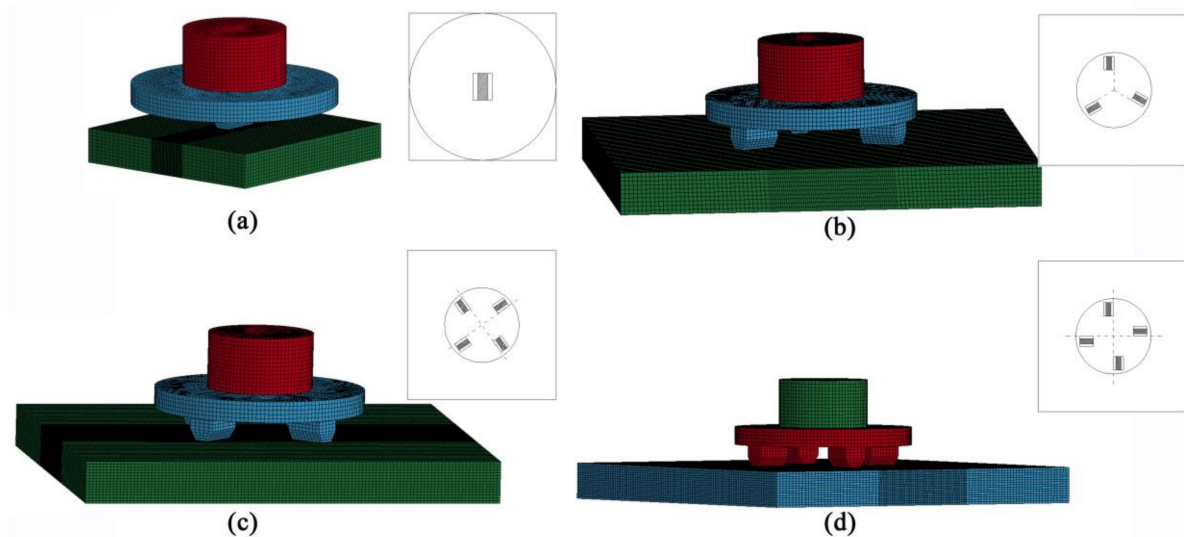

Figure 2. Numerical model for impact tests of concrete slabs. (**a**) Single impact head; (**b**) Three impact head; (**c**) Long axis of four impact heads along the diagonal direction (condition I); (**d**) Long axis of four impact heads along the symmetry axis direction (condition II).

Table 1. Material model properties of the hammer, bearing plate, impact head, and concrete slab.

Parameters	Hammer, Bearing Plate, and Impact Head	Concrete Slab
Density (kg/m^3)	7850	2400
Young's modulus (GPa)	200	28
Poisson's ratio	0.25	0.2
Uniaxial compressive strength (MPa)		40
Tensile strength (MPa)		5

Table 2. Impact test parameters of a single impact head.

Concrete Slab Size (mm)	Impact Velocity (m/s)	Drop Hammer Weight (kg)
	3	10
300 × 300 × 50	4	10
	5	10
	4	17
300 × 300 × 80	5	17
	6	17

Table 3. Impact test parameters of a multi-impact head.

Concrete Slab Size (mm)	Drop Height (mm)	Drop Hammer Weight (kg)
500 × 500 × 60	600	10
600 × 600 × 60	800	10
700 × 700 × 60	1000	10

2.2. Failure Criterion

For the simulation of low-velocity impact tests on concrete slabs using LS-DYNA 19.0 developed by Livermore Software Technology Corporation (Livermore, CA, USA), the

Winfrith (MAT84) concrete constitutive model, with relatively few model parameters, was selected by referring to the research results of others [16–19]. This model was developed by Broadhouse in the 1980s [22,23], and the plastic shear failure adopts the following Ottosen four-parameter mode:

$$Y(I_1, J_2, J_3) = \alpha J_2 + \lambda \sqrt{J_2} + bI_1 - 1 \tag{1}$$

$$\lambda \begin{cases} k_1 \cos\left[\frac{1}{3} \cos^{-1}(k_2 \cos(3\theta))\right] & \cos(3\theta) \geq 0 \\ k_1 \cos\left[\frac{\pi}{3} - \frac{1}{3} \cos^{-1}(-k_2 \cos(3\theta))\right] & \cos(3\theta) \leq 0 \end{cases} \tag{2}$$

$$\cos(3\theta) = \frac{3\sqrt{3}}{2} \frac{J_3}{J_2^{3/2}} \tag{3}$$

where the four parameters a, b, k_1, and k_2 are all functions of the ratio of tensile to compressive strength (f_t/f'_c), which can be determined by uniaxial tension ($\theta = 60°$), uniaxial compression ($\theta = 0°$), biaxial compression ($\theta = 0°$), and triaxial compression ($\theta = 60°$).

Since the Winfrith model does not define tensile failure, MAT_ADD_EROSION was added to define material failure [24,25]. Under impact, the strength of concrete changes with the strain rate, which mainly produces compressive failure. Therefore, the principal strain was used as the failure criterion for the concrete materials. Concrete usually shows tensile failure or shear failure, in which the hydrostatic pressure is positive for pressure and negative for tension; therefore, hydrostatic pressure failure was used to give the minimum pressure that the concrete could withstand. If the hydrostatic pressure was less than the minimum pressure, then the material would fail.

3. Results and Discussion

3.1. Crack Development Law under a Single Impact Head

The 300 × 300 × 50 mm concrete slab was cracked by the single impact head. The crack propagation mode of the concrete slab is shown in Figure 3 for the drop hammer impact velocities of 3 m/s, 4 m/s, and 5 m/s. At the impact velocity of 3 m/s, a compression-shear failure zone appeared on the top of the concrete slab. The failure zone was located at the impact position of the impact head, with the stress at the vertex of the rectangular impact head being larger, and short micro-cracks appeared at the bottom of the concrete slab. When the impact velocity was 4 m/s, the stress concentration area on the top of the impact head expanded along the long axis, there was an obvious stress concentration near the long side of the rectangular impact head, and the cracks at the bottom of the concrete slab were along the long axis of the impact head. When the impact velocity was 5 m/s, the compression shear failure area on the top of the concrete slab displayed obvious damage, and the main crack ran up and down along the thickness direction of the slab and then ran through the concrete slab along the long axis of the impact head.

The 300 × 300 × 80 mm concrete slab was also cracked by the single impact head. The crack propagation mode of the concrete slab is shown in Figure 4 for the drop hammer impact velocities of 4 m/s, 5 m/s, and 6 m/s. At the impact velocity of 4 m/s, there was a stress concentration around the impact head, and a compression shear area appeared; however, there was no obvious damage at the bottom of the concrete slab. When the impact velocity was 5 m/s, the penetration depth of the top compressive shear failure zone on the concrete slab increased, and the main crack ran through the concrete slab along the long axis of the impact head. In addition to the main crack running through the bottom of the concrete slab, there were also tiny short cracks in the center of the slab bottom. Under the impact velocity of 6 m/s, the stress concentration area at the top of the concrete slab was mainly located directly below the impact head, the penetration depth increased, and the width of the main crack through the concrete slab increased.
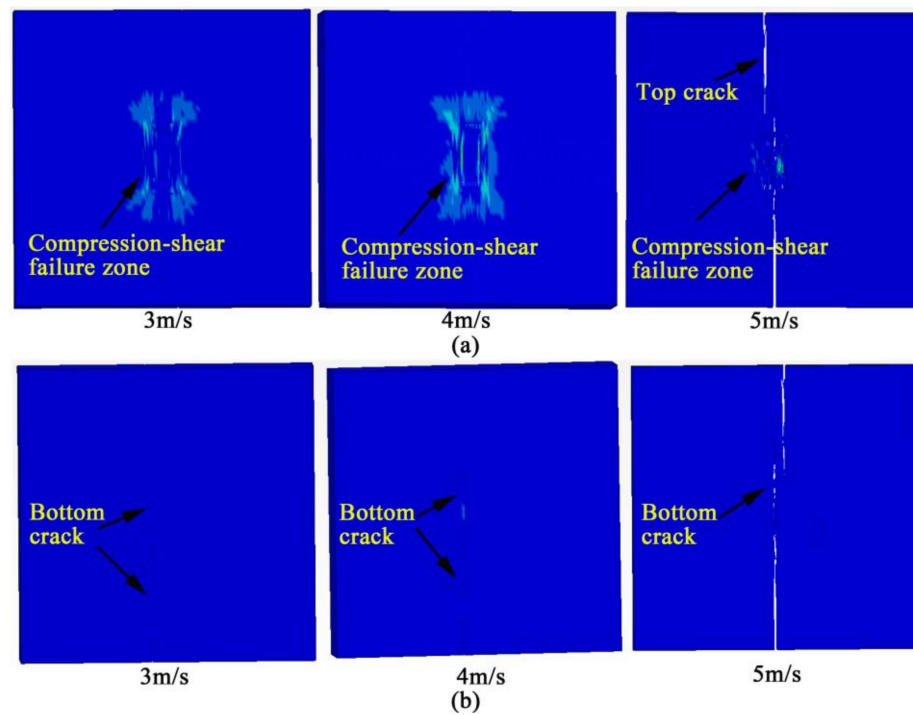
Figure 3. Crack propagation of 50 mm concrete slab. (**a**) Top surfaces; (**b**) Bottom surfaces.
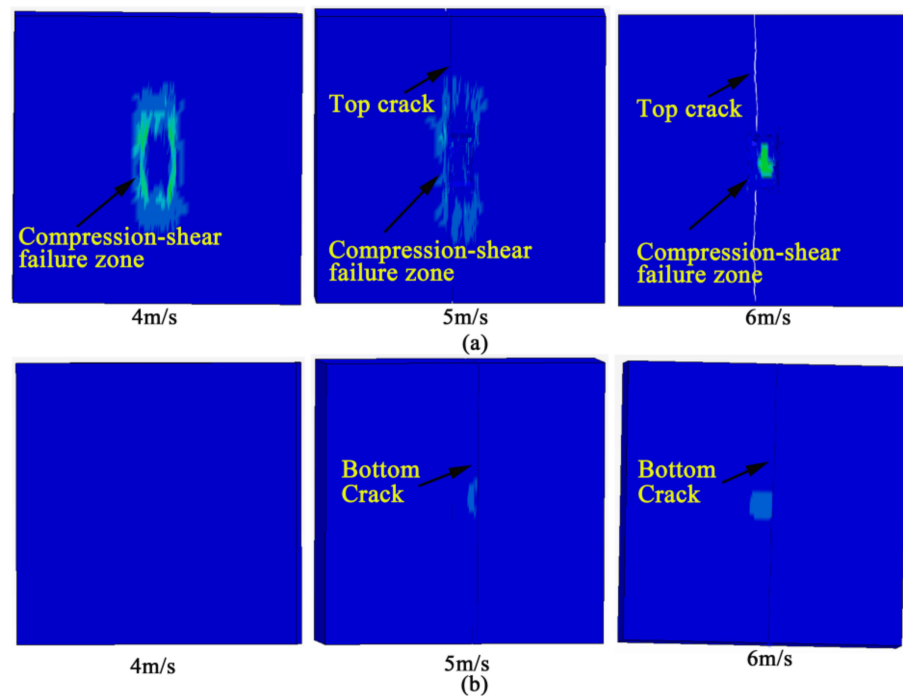

Figure 4. Crack propagation of 80 mm concrete slab. (**a**) Top surfaces; (**b**) Bottom surfaces.

The simulation results of the impact fractures using the single impact head showed that fractures of concrete slabs mainly included compression shear failure of the impact core and tensile failure of the main crack. Under the impact load, stress concentration appeared on the four sides and vertices of the rectangular impact head. When the main crack expanded and the penetration depth of the compression shear zone increased, the stress concentration mainly existed in the compression shear zone. The main crack first appeared at the bottom of the concrete slab. With an increase in the impact height, the crack extended from the bottom of the slab to the top of the concrete slab until it ran through

the concrete slab along the long axis of the impact head, and the specimen failed. The simulation test results are in good agreement with those of the indoor tests.

3.2. Crack Development Law and Cracked Core Morphology of Multi-Impact Heads

In the impact tests with three impact heads, the fracture morphology of three types of concrete slabs with dimensions of 500 × 500 × 60 mm, 600 × 600 × 60 mm, and 700 × 700 × 60 mm at impact heights of 600 mm, 800 mm, and 1000 mm are shown in Figures 5–7.

Figure 5. Fracture morphology of 500 × 500 × 60 mm concrete slab under three impact heads. (**a**) Impact height 600 mm; (**b**) Impact height 800 mm; (**c**) Impact height 1000 mm.
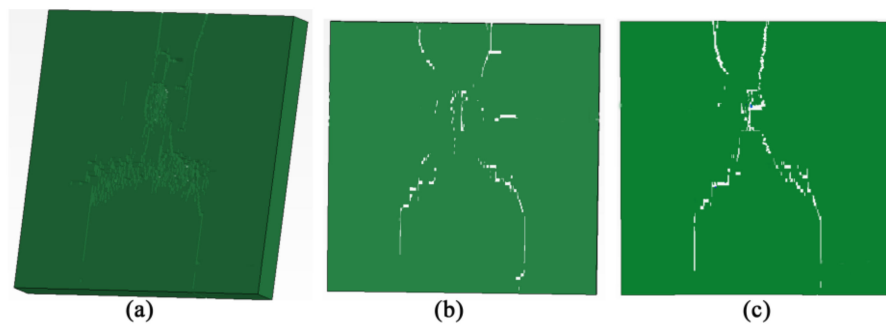
Figure 6. Fracture morphology of 600 × 600 × 60 mm concrete slab under three impact heads. (**a**) Impact height 600 mm; (**b**) Impact height 800 mm; (**c**) Impact height 1000 mm.

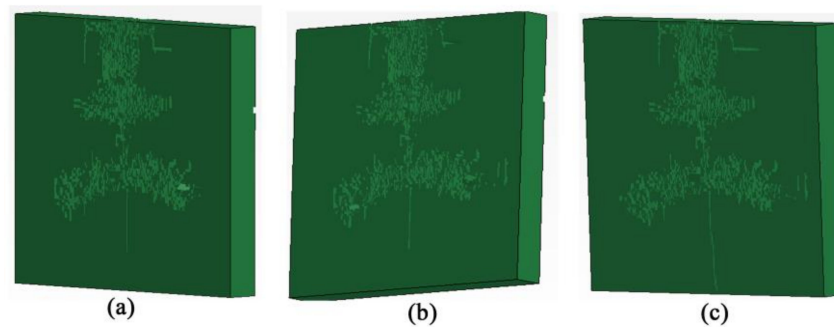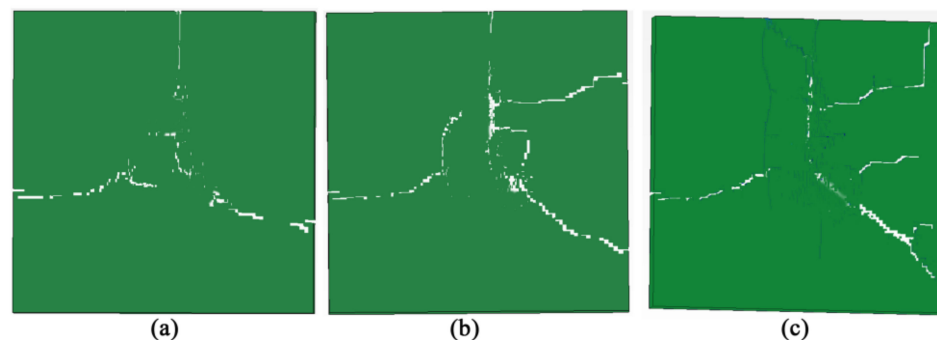**Figure 7.** Fracture morphology of 700 × 700 × 60 mm concrete slab under three impact heads. (**a**) Impact height 600 mm; (**b**) Impact height 800 mm; (**c**) Impact height 1000 mm.

As shown in Figure 5, after the impact cracking of the 500 × 500 × 60 mm concrete slab, there was an obvious compression-shear failure zone at the impact head position, and the crack expanded along the long axis of the impact head. The direction of the long axis of one of the impact heads was the same as the direction of the symmetry axis of the concrete slab. Due to the relatively small size of the concrete slab, cracks would rapidly develop along the long axis of the other impact heads after they appeared. After the impact

cracking of the 600 × 600 × 60 mm concrete slab, at the impact head position where the long axis direction was consistent with the symmetry axis of the concrete slab, multiple cracks developed along the long axis direction to the edge of the concrete slab, as shown in Figure 6. Along the oblique direction of the long axes of the other two impact heads, the crack propagated until it reached the edge of the concrete slab, and a triangular-like cracked core was generated in the center of the concrete slab. As shown in Figure 7, after the 700 × 700 × 60 mm concrete slab was cracked, cracks were more likely to develop along the long axis of each impact head because the size of the concrete slab was relatively large and the impact head was far away from the edge of the concrete slab. When the impact height was low, an approximately triangular cracked core appeared in the center of the concrete slab. With an increase in the impact height, the main cracks met in the concrete slab, and at this time, multiple cracks expanded along the short axis of the impact head.

Under the condition of impact cracking with four impact heads, and with the long axis of the impact head located in the diagonal direction of the concrete slab (Condition I), the fracture morphology of three types of concrete slabs with dimensions of 500 × 500 × 60 mm, 600 × 600 × 60 mm, and 700 × 700 × 60 mm at impact heights of 600 mm, 800 mm, and 1000 mm are shown in Figures 8–10.

Figure 8. Fracture morphology of 500 × 500 × 60 mm concrete slab under four impact heads (Condition I). (**a**) Impact height 600 mm; (**b**) Impact height 800 mm; (**c**) Impact height 1000 mm.

Figure 9. Fracture morphology of 600 × 600 × 60 mm concrete slab under four impact heads (Condition I). (**a**) Impact height 600 mm; (**b**) Impact height 800 mm; (**c**) Impact height 1000 mm.

As shown in Figure 8, after the impact cracking of the 500 × 500 × 60 mm concrete slab, the cracks were mainly concentrated in the core position of the concrete slab and the cracks in the direction of the impact head formed an approximately quadrilateral cracked core. Due to the relatively small size of the concrete slab, the cracks spread along the connecting line of the two opposite impact heads, and there were many micro-cracks in the concrete slab locally. After the impact cracking of the 600 × 600 × 60 mm concrete slab, as shown in Figure 9, an approximately quadrilateral cracked core was formed in the center of the slab. The crack developed not only in the direction of the connecting line between the two opposite impact heads, but also in the direction of the connecting line between the two adjacent impact heads. The higher the impact height was, the more obvious the produced

quadrilateral cracked core was. As shown in Figure 10, after the impact cracking of the 700 × 700 × 60 mm concrete slab, the impact-cracked core of the concrete slab was obvious, and a quadrilateral cracked core appeared under the conditions of different impact heights. When the impact height was increased, the cracks at the connecting line of the cracked core were more significant and developed towards the edge of the concrete slab.
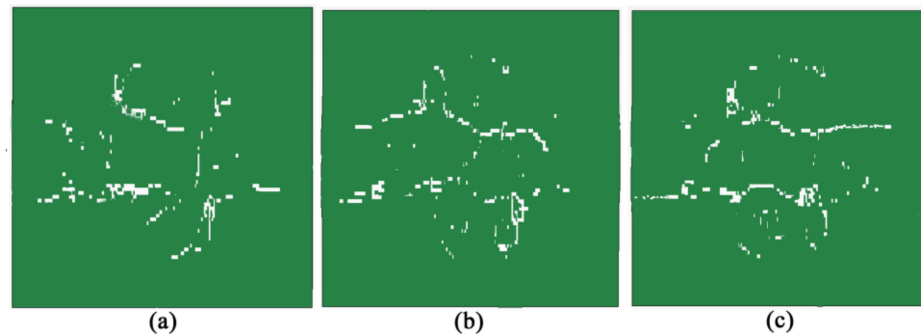

Figure 10. Fracture morphology of 700 × 700 × 60 mm concrete slab under four impact heads (Condition I). (**a**) Impact height 600 mm; (**b**) Impact height 800 mm; (**c**) Impact height 1000 mm.
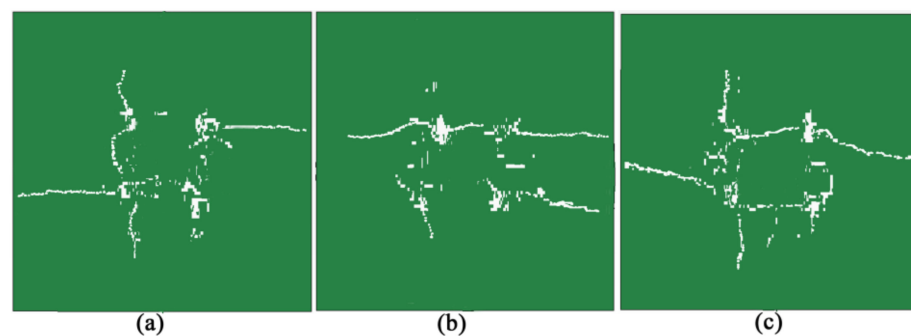
Under four impact heads with working Condition II, the position of the impact heads relative to the concrete slab was changed; the connecting line of the long axes of the two opposite impact heads was along the direction of the symmetry axis of the concrete slab. Figures 11–13 show the fracture morphology of the three types of concrete slabs (500 × 500 × 60 mm, 600 × 600 × 60 mm, and 700 × 700 × 60 mm) under the conditions of 600 mm, 800 mm, and 1000 mm impact heights.

Figure 11. Fracture morphology of 500 × 500 × 60 mm concrete slab under four impact heads (Condition II). (**a**) Impact height 600 mm; (**b**) Impact height 800 mm; (**c**) Impact height 1000 mm.

Figure 12. Fracture morphology of 600 × 600 × 60 mm concrete slab under four impact heads (Condition II). (**a**) Impact height 600 mm; (**b**) Impact height 800 mm; (**c**) Impact height 1000 mm.
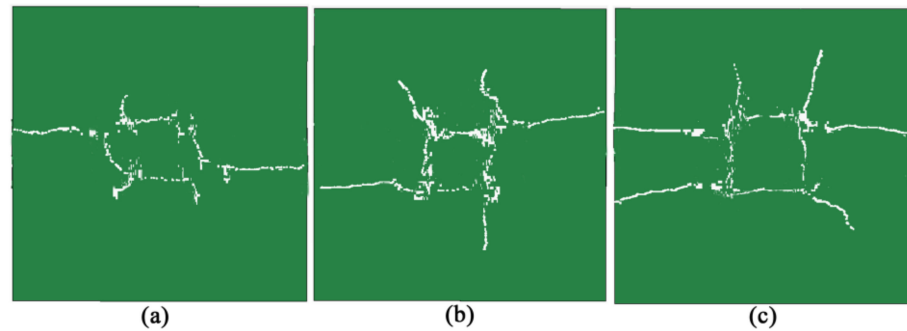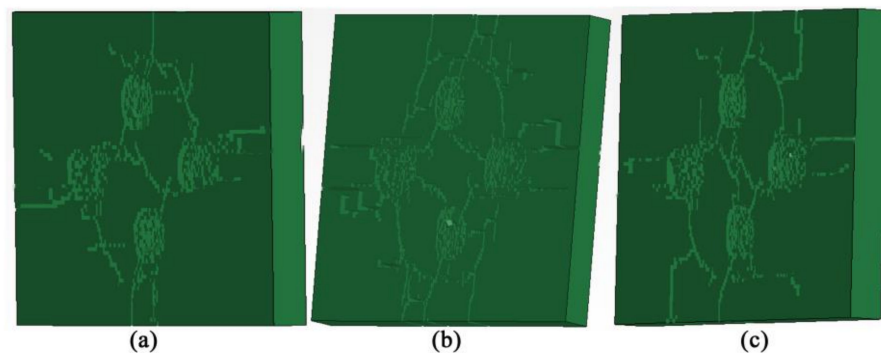
Figure 13. Fracture morphology of 700 × 700 × 60 mm concrete slab under four impact heads (Condition II). (**a**) Impact height 600 mm; (**b**) Impact height 800 mm; (**c**) Impact height 1000 mm.
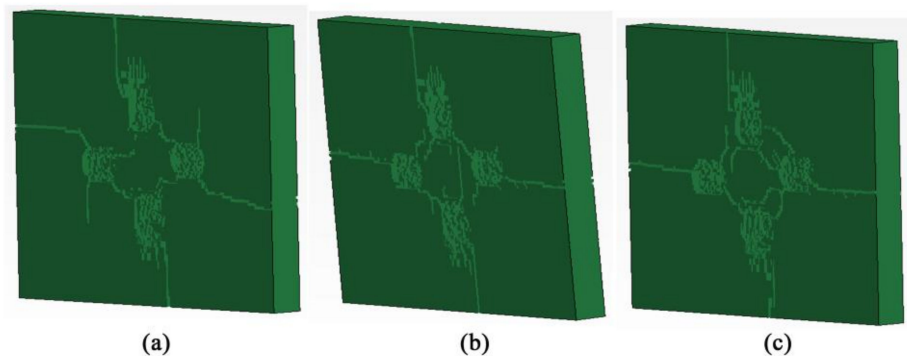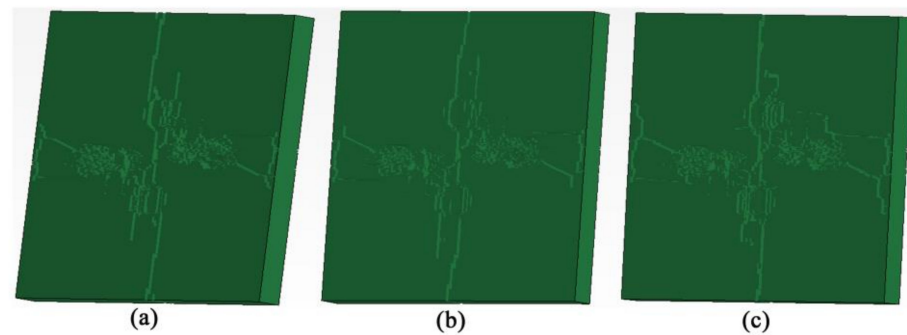
After the impact cracking of the 500 × 500 × 60 mm concrete slab, as shown in Figure 11, a cracked core appeared in the center of the concrete slab. The cracked core was approximately quadrilateral, and the crack developed along the line connecting the two adjacent impact heads. Due to the relatively small size of the concrete slab, the cracks in the core area developed abundantly, and the cracks extended outward to the edge of the concrete slab. As shown in Figure 12, after the 600 × 600 × 60 mm concrete slab was cracked, an approximately quadrilateral cracked core appeared in the center of the concrete slab. The cracks of the cracked core developed along the line connecting the rectangular vertices of the adjacent impact heads, and the cracked core was perpendicular to the diagonal of the concrete slab. When the impact height was increased, cracks would appear again in the direction of the connecting line of the impact heads, at the outer edge of the cracked core. In the direction of the long axis of the impact heads, the cracks spread outward along the normal direction of the four sides of the concrete slab until they reached the edge of the concrete slab. As shown in Figure 13, after the 700 × 700 × 60 mm concrete slab was cracked, the cracks not only developed along the line connecting the two adjacent impact heads, but also extended along the line connecting the opposite impact heads. In addition to the cracks on the four sides of the rupture core, there were also cross cracks in the center of the slab. Along the long axis of the impact heads, a number of cracks extended outward to the edge of the concrete slab, and also intersected with the cracks in the short axis direction of the adjacent impact heads to form cracked blocks.

The multi-impact head fracture test showed that a cracked core formed in the center of the concrete slab. In the three-impact-head impact tests, the crack first developed along the long axis of the impact head, and the expansion of the three main cracks usually formed an approximately triangular cracked core in the concrete slab. After the cracked core was formed, the main cracks developed to the edge of the slab. At this time, in addition to the three main cracks, one or two branch cracks appeared outside the cracked core and developed towards the slab edge. In the impact tests of four impact heads, when the direction of the long axis of the impact heads was along the diagonal direction of the concrete slab (Condition I), a nearly quadrilateral cracked core appeared in the concrete slab, with the four sides of the cracked core being parallel to the four sides of the concrete slab. With an increase in the impact height, the cracks in the cracked core zone expanded to the edge of the concrete slab. When the position of the four impact heads was changed relative to the concrete slab so that the long axis of the impact head was along the symmetry axis of the concrete slab (Condition II), the concrete slab also developed an approximately quadrilateral cracked core, but the four sides of the cracked core were perpendicular to the diagonal of the concrete slab. With an increase in the impact height, the cracked core zone expanded outward, and cross cracks appeared in some core areas. Similar to the three impact heads, under the impact of four impact heads, several branch cracks appeared after the cracked core was formed. However, the difference was that, for the concrete slab continuously impacted by four impact heads, the four main cracks of the cracked core

developed to the edge of the slab, whereas the branch cracks rarely developed to the edge of the concrete slab.

3.3. Comparative Analysis of Fracture Law with Indoor Low-Velocity Impact Tests

In the indoor low-velocity impact tests on concrete slabs, under impact-cracking conditions using a single impact head, three impact heads, and four impact heads (Condition I), the concrete slab failed. The crack development is shown in Figure 14.

Figure 14. Fracture forms of concrete slabs impacted by different impact heads. (**a**) Single impact head; (**b**) Three impact heads; (**c**) Four impact heads (condition I).

In the indoor tests of low-velocity impact cracking of concrete slabs, under the low-velocity impact of a single impact head, there was a compressive shear failure zone on top of the concrete slab regardless of whether the concrete slab was 50 mm thick or 80 mm thick. The bottom of the concrete slab first cracked, the crack developed upwards until the main crack ran through the concrete slab, and then the concrete slab specimen failed [9]. When three impact heads were used for impact tests, the initial crack appeared at the bottom of the concrete slab; the crack first extended forward along a main crack, and then multiple branch cracks appeared. When the concrete slab finally failed, a triangular fracture core was usually formed in the center of the slab. Under the impact of four impact heads (Condition I), the bottom of the concrete slab cracked first, and a nearly quadrilateral fracture core generally appeared in the center of the concrete slab, while the top surface of the concrete slab cracked at a later time than the bottom. The sides of the cracked core were approximately parallel to the edge of the concrete slab, and cracks appeared along the long axis of the impact head and developed to the edge of the concrete slab.

Through numerical simulation, the crack propagation forms of concrete slabs under the conditions of a single impact head, three impact heads, and four impact heads were analyzed. Figure 15 shows the failed concrete slabs of a single impact head, three impact heads, and four impact heads (Condition I). Under the impact of the single impact head, cracks first appeared at the bottom of the concrete slab, a compression shear zone appeared on the top of the slab, and stress concentration appeared on the four sides and vertices of the impact head. Cracks at the bottom of the concrete slab extended to the top of the slab, and when the main crack ran through the concrete slab, the concrete slab failed. At this time, the stress concentration around the impact head dissipated; however, the stress concentration mainly occurred in the compression-shear zone just below the impact head. Under the impact of three impact heads, the crack first developed along the long axis of each impact head. Due to the stress concentration at the vertex of the rectangular impact head, the fracture first occurred at the vertex; then, cracks expanded along the shortest distance from the adjacent vertex of the impact head, and finally, a triangular cracked core was formed. Cracks also appeared in the long axis direction of the outer edge of the impact head until the cracks developed to the edge of the concrete slab, causing the specimen to fail. Four impact heads were used to impact the concrete slab, with the long

axis of the impact head being along the diagonal direction of the concrete slab (Condition I). When the concrete slab failed, a quadrangular fracture core was formed in the center of the concrete slab. The four sides of the cracked core were approximately parallel to the edges of the concrete slab. The cracks in the cracked core developed to the edge of the slab, and some cracks extended to the edge of the concrete slab. At this time, the specimen would have failed.
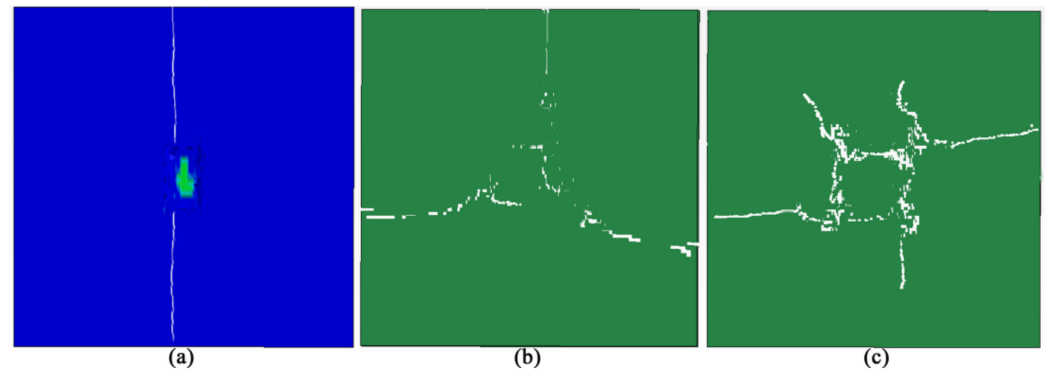

Figure 15. Numerical results of concrete slabs impacted by different impact heads. (**a**) Single impact head; (**b**) Three impact heads; (**c**) Four impact heads (condition I).

3.4. Discussion

The numerical simulation results were consistent with the indoor test results [9]. Under the failure condition of a single impact head, the concrete slab first cracked at the bottom; at the same time, a compressive shear failure zone appeared at the impact position on the top of the slab. Meanwhile, the main crack developed along the long axis of the impact head. The main crack ran through the concrete slab, and the concrete slab specimen was damaged. When three or four impact heads were used, the rupture core was formed in the impact center of the concrete slab. Three impact heads generated a triangular rupture core, and four impact heads generated a quadrangular rupture core. Similar to the research results of Nia, Hedayatian, and Nili et al. [10], the numerical simulation results were basically consistent with the indoor test results. Under the condition of a single impact head fracture, the concrete slab first cracked at the bottom, and the compression shear failure zone appeared at the impact position on the top of the slab. The main crack developed along the long axis of the single impact head. With the main crack running through the concrete slab, the concrete slab specimen failed. When three or four impact heads were used, the cracked core formed in the impact center of the concrete slab; three impact heads generated a triangular ruptured core, and four impact heads generated a quadrangular cracked core.

4. Optimization of Homogenized Micro-Crack Crushing Hammer

4.1. Research on In Situ Micro-Crack Homogenization of Concrete Pavement

When the old concrete pavement was micro-cracked and homogenized, the impact crushing was carried out along the driving direction of the road. After each impact of the drop hammer, an approximately quadrilateral cracked core was generated in the impact core area. When two impact areas were adjacent or partially overlapping, the cracks in the cracked core along the driving direction passed through and developed rapidly along the driving direction. If the local bearing capacity of concrete pavement is insufficient, or the strength of a concrete slab is insufficient, it is easy to generate longitudinal reflection cracks in the corresponding positions after the asphalt pavement is overlaid. In order to reduce the occurrence of such problems, the crushing process was initially improved, and the crushing of concrete pavement was changed from the original no-spacing impact to a one-hammer impact, as shown in Figure 16.
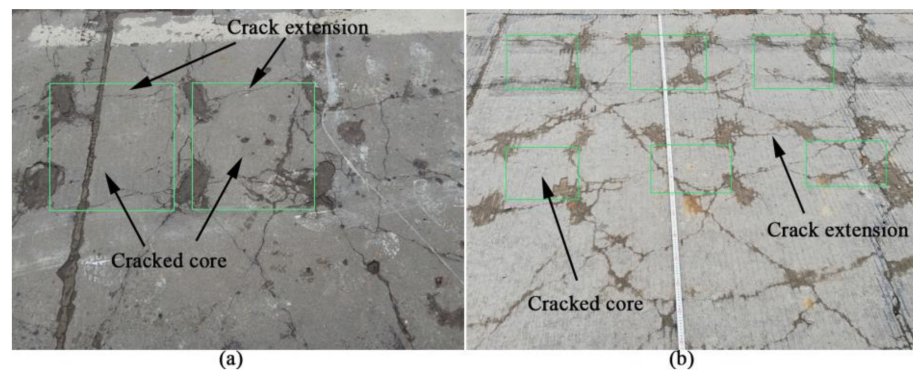
Figure 16. Crushing effect of continuous and interval one-step impacts. (**a**) Continuous impact; (**b**) Interval one step impact.

When the concrete pavement was crushed at intervals of one hammer, the cracks of the quadrilateral cracked core along the driving direction still extended. Although the cracks at some positions were not fully connected, they might have been connected with each other under the road traffic load, and longitudinal reflection cracks might have occurred after the asphalt pavement was overlaid.

In order to solve the longitudinal crack extension problem caused by the cracked core at the local road position after crushing, the construction process was adjusted again, as shown in Figure 17. During homogenized micro-crack crushing, a cement concrete panel was divided into three columns, which increased the transverse spacing of the impact area of the drop hammer, and the impact positions between different columns were staggered with each other. The interval of each broken column was two hammers to reduce the extension probability of longitudinal cracks in the cracked core. Increasing the distance between hammers effectively reduced the longitudinal crack extension caused by the cracked core. However, due to the large distance between impact areas, the fragmentation of the concrete pavement after crushing the slab was large and the fracture blocks were uneven. Uneven fracture blocks of concrete pavement are known to cause uneven bearing capacity, as there is a large difference in the expansion and contraction of fracture blocks due to temperature changes. Under traffic load and temperature load, reflective cracking also commonly occurs after the asphalt pavement is overlaid. In order to better solve the problem of longitudinal extension cracks caused by an impact-cracked core, it is necessary to further study the construction technology and fracture equipment.

Figure 17. Crushing effect of interval two-step impacts.

4.2. Optimization of Homogenized Micro-Crack Crushing Hammer

In the numerical simulation of low-velocity impact tests, when four impact heads were used to impact and crush the concrete slab, the impact head rotated at a certain angle and the cracks in the concrete slab appeared in different propagation modes, as shown in Figure 18. When the long axis of the impact head was located in the diagonal direction of

the concrete slab (Condition I), the sides of the cracked core were approximately parallel to the edges of the concrete slab. There were cracks on the outside of the apex of the impact heads, which developed obliquely along the long axis of the impact heads until the slab failed. Relative to the concrete slab, when the impact heads rotated 45° along the centroid, the quadrilateral cracked core also rotated 45°, and the four sides of the cracked core were perpendicular to the diagonal of the concrete slab (Condition II). The crack on the outside of the impact head developed along the long axis until reaching the edge of the slab, and then the slab failed. It can be seen that, due to the overall rotation of the impact heads, the crack propagation morphology in the middle and outer edges of the concrete slab was changed.

(a) (b)
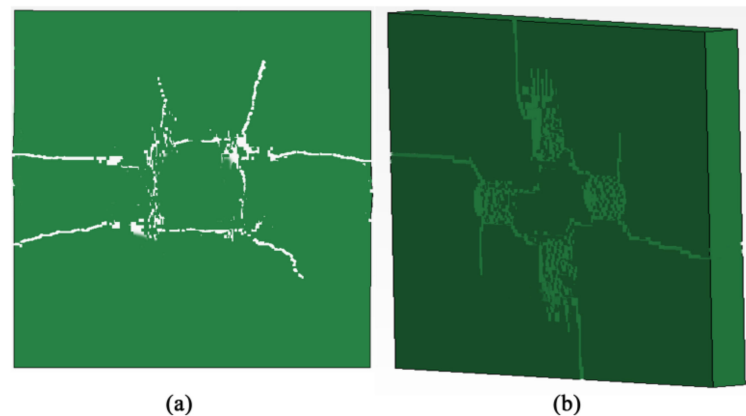
Figure 18. Fracture forms of concrete slab under four impact heads with two conditions. (**a**) Four impact heads (condition I); (**b**) Four impact heads (Condition II).

In order to solve the problem of longitudinal crack extension of the fracture core at local locations on the road, the longitudinal cracking between hammers can be reduced by adjusting the impact spacing of drop hammers based on the original hammer structure. However, if the hammer crushing distance is too large, the pavement slab will not crack completely, and with changes in the external temperature there will be excessive shrinkage and deformation, which is likely to cause the occurrence of reflection cracks in the asphalt overlay.

On the basis of ensuring the homogenized micro-crack crushing effect of concrete slabs, and in order to effectively solve the problem of longitudinal cracks, the distribution of the impact heads of the hammer was improved to a certain extent. The results of the analysis are shown in Figure 19.
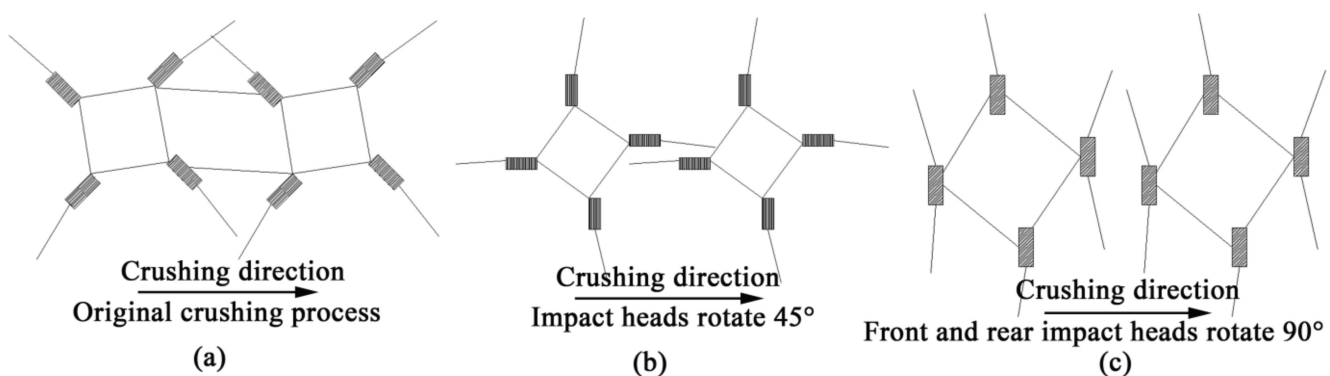

(a) (b) (c)

Figure 19. Optimization analysis on the distribution of hammer impact head. (**a**) Original method; (**b**) Improved method I; (**c**) Improved method II.

The results of the field tests, indoor tests, and numerical simulations show that a quadrilateral cracked core will be generated under the impact crushing of four impact

heads, and the distribution of impact heads will affect the shape of the cracked core. When the original drop hammer was used for crushing along the driving direction, the cracks in the cracked core along the driving direction were easy to extend and connect. If the drop hammer was rotated by 45°, the quadrilateral cracked core also rotated by 45°. At that time, the cracks in the quadrilateral cracked core could not extend forward and backward, which effectively prevented the generation of longitudinally extending cracks. Since the cracks mainly developed along the long axis of the impact head, the longitudinal cracks generated by the front and rear impact heads along the construction direction may have connected with each other. On the basis of a 45° rotation of the hammer body, the front and rear impact heads rotated 90 ° again. Although the four sides of the cracked core still intersected obliquely with the driving direction, the crack could not extend and expand, because the crack still developed along the long axis of the front and rear impact heads; therefore, the cracks crushed by the front and rear impact heads did not extend and connect.

Under the condition of insufficient test conditions, the numerical simulation method can be used to carry out research first, so as to provide a basis for subsequent field tests [17]. In order to verify the theoretical analysis, an impact fracture simulation study was carried out on the drop hammer before and after improvement. The size of the concrete slab was $1000 \times 1000 \times 60$ mm, and impact crushing of the slab was carried out along the driving direction, with an interval of two columns, a total of four times. The crack expansion is shown in Figure 20. Under the impact of the original drop hammer, each impact area formed a quadrilateral cracked core, and the cracks in the cracked core along the construction direction were approximately parallel to the edge of the concrete slab. Meanwhile, the cracks extended forward and finally connected with each other. After the drop hammer with the four impact heads rotated by 45°, the cracked core also rotated by approximately 45°. The cracks in the cracked core did not expand or extend, but longitudinally expanding micro-cracks appeared at the front and rear impact heads along the construction direction. When the front and rear impact heads were rotated by 90°, the shape of the cracked core was basically unchanged, but the longitudinal micro-cracks of the front and rear impact heads were perpendicular to the driving direction and would not continue to extend or intersect.
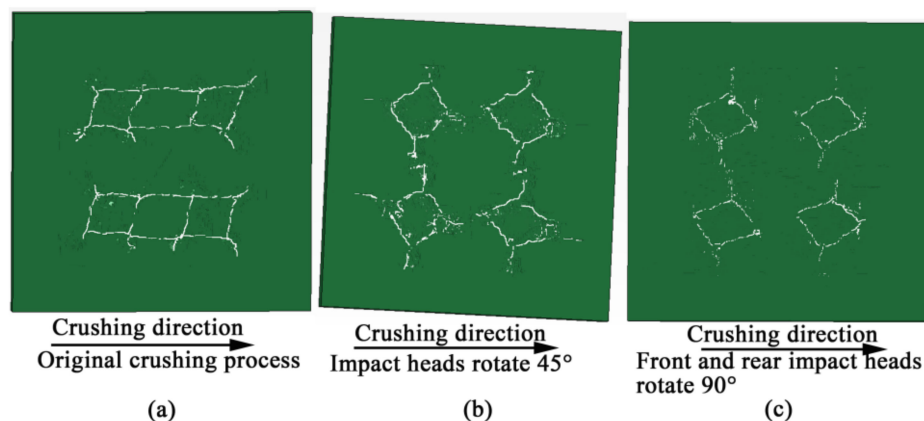

Figure 20. Fracture forms of concrete slabs under three kinds of hammer impacts. (**a**) Original method; (**b**) Improved method I; (**c**) Improved method II.

The indoor test and numerical simulation results showed that the cracks mainly developed along the long axis of the four impact heads. Because the four vertices of the rectangular impact head generated a large stress concentration, the cracks usually started at the vertices of the impact head, forming a quadrilateral cracked core. The cracks of the cracked core were easy to extend and connect along the driving direction, forming a longitudinal extension joint, and reflective cracking occurred easily after overlaying with asphalt pavement. In view of this, through the optimal layout of hammer impact heads, the problem of longitudinal crack extension of cracked cores can be effectively solved so as to reduce the probability of longitudinal reflection cracks in asphalt pavement. However, in

order to verify the rationality of the optimization of the hammer impact head layout and its practical application in engineering, field test research will be carried out in the follow-up.

5. Conclusions

In this paper, the crack propagation mode of concrete slabs under low-velocity impacts using different numbers and distributions of impact heads was studied through numerical simulation, and then the numerical simulation results were compared with those of indoor low-velocity impact tests to verify the rationality of the simulation. Finally, according to the field test results, the layout of the drop hammer impact heads was optimized using numerical simulation. The main conclusions are as follows:

Under the impact crushing of a single impact head, the compression shear failure zone appeared on the top surface of the concrete slab, and a large stress concentration appeared at the four vertices and sides of the rectangular impact head. Cracks first appeared at the bottom of the concrete slab, and then the main cracks developed upwards until they ran through the concrete slab.

In the multi-impact head fracture tests, a cracked core was formed in the center of the concrete slab. When three impact heads were used, the geometry of the cracked core of the concrete slab was approximately triangular; however, when four impact heads were used, the geometry of the fracture core was approximately quadrilateral. Compared with branch cracks, the main cracks of the cracked cores were more likely to propagate to the edge of the concrete slab. Moreover, the crack development and final fracture state of the concrete slab was affected by the size of the slab.

The numerical simulation results of low-velocity impact tests showed a good agreement with the experimental data; therefore, it seems that the numerical method can predict low-velocity impact test results with an acceptable accuracy.

The optimal layout of drop hammer impact heads as determined by numerical simulation not only ensured the homogenized micro-crack crushing effect of the concrete pavement, but also effectively solved the problem of longitudinal crack extension of the cracked core, so as to effectively avoid the generation of longitudinal reflection cracks in the asphalt overlay. However, further field tests should be carried out to evaluate the rationality of the numerical simulation on the layout optimization of hammer impact heads in actual concrete pavement rehabilitation.

References

1. Xu, Z.J.; Ling, J.M.; Hung, Q.L. Research on resonant rubblized effects of PCC pavement. *China J. Highw. Transp.* **2008**, *21*, 26–32. (In Chinese)
2. Ma, J.; Sun, S.Z.; Rui, H.T.; Wang, L.; Ma, Y.; Zhang, W.W.; Zhang, W.; Liu, H.; Chen, H.Y.; Liu, J.; et al. Review on China's road construction machinery research progress: 2018. *China J. Highw. Transp.* **2018**, *21*, 136–139. (In Chinese)
3. Liu, L.; Wu, S.H.; Xie, W.K.; Yao, G. Numerical analysis of rehabilitated concrete pavement using crack-and-seating technique. *Int. J. Pavement Eng.* **2021**, *22*, 1250–1262. [CrossRef]

4. Chen, C.; Lin, S.; Williams, R.C.; Ashlock, J.C. Non-destructive modulus testing and performance evaluation for asphalt pavement reflective cracking mitigation treatments. *Balt. J. Road Bridge Eng.* **2018**, *13*, 46–53. [CrossRef]

5. Ceylan, H.; Gopalakrishnan, K.; Coree, B.J.; Kota, T.; Mathews, R. Rehabilitation of concrete pavements utilizing rubblization: A mechanistic based approach to HMA overlay thickness design. *Int. J. Pavement Eng.* **2008**, *9*, 45–57. [CrossRef]

6. Chen, D.H.; Huang, Q.L.; Ling, J.M. Shanghai's Experience on Utilizing the Rubblization for Jointed Concrete Pavement Rehabilitation. *J. Perform. Constr. Facil.* **2008**, *22*, 398–407. [CrossRef]

7. Qiu, X.; Ling, J.M.; Wang, F. Concrete pavement rehabilitation procedure using resonant rubblization technology and mechanical-empirical based overlay design. *Can. J. Civ. Eng.* **2014**, *41*, 32–39. [CrossRef]

8. Ge, Z.S.; Li, H.; Han, Z.T.; Zhang, Q.S. Properties of cold mix asphalt mixtures with reclaimed granular aggregate from crushed PCC pavement. *Constr. Build. Mater.* **2015**, *77*, 404–408. [CrossRef]

9. Li, W.J.; Zhang, Q.L.; Zhi, Z.H.; Feng, C.; Cai, Y.C.; Yue, J.C. Investigation on the fracture mechanism of homogenized micro-crack crushing technology for portland cement concrete pavement rehabilitation. *AIP Adv.* **2019**, *9*, 075113. [CrossRef]

10. Nia, A.A.; Hedayatian, M.; Nili, M.; Sabet, V.A. An experimental and numerical study on how steel and polypropylene fibers affect the impact resistance in fiber-reinforced concrete. *Int. J. Impact Eng.* **2012**, *46*, 62–73.

11. Sakthivel, P.B.; Ravichandran, A.; Alagamurthi, N. Impact strength of hybrid steel mesh-and-fiber reinforced cementitious composites. *KSCE J. Civ. Eng.* **2015**, *19*, 1385–1395. [CrossRef]

12. Yahaghi, J.; Muda, Z.C.; Beddu, S.B. Impact resistance of oil palm shells concrete reinforced with polypropylene fibre. *Constr. Build. Mater.* **2016**, *123*, 394–403. [CrossRef]

13. Elavarasi, D.; Mohan, K.S.R. On low-velocity impact response of SIFCON slabs under drop hammer impact loading. *Constr. Build. Mater.* **2018**, *160*, 127–135. [CrossRef]

14. Othman, H.; Marzouk, H. An experimental investigation on the effect of steel reinforcement on impact response of reinforced concrete plates. *Int. J. Impact Eng.* **2016**, *88*, 12–21. [CrossRef]

15. Othman, H.; Marzouk, H. Impact response of ultra-high-performance reinforced concrete plates. *ACI Struct. J.* **2016**, *113*, 1325–1334. [CrossRef]

16. Xiao, Y.; Li, B.; Fujikake, K. Behavior of Reinforced Concrete Slabs under Low-Velocity Impact. *ACI Struct. J.* **2017**, *114*, 643–658. [CrossRef]

17. Yoo, D.Y.; Yoon, Y.S. Influence of steel fibers and fiber-reinforced polymers on the impact resistance of one-way concrete slabs. *J. Compos. Mater.* **2014**, *48*, 695–706. [CrossRef]

18. Ganesan, P.; Kumar, S.V.S. FE modelling of low velocity impact on RC and prestressed RC slabs. *Struct. Eng. Mech.* **2019**, *71*, 515–524.

19. Anil, O.; Kantar, E.; Yilmaz, M.C. Low velocity impact behavior of RC slabs with different support types. *Constr. Build. Mater.* **2015**, *93*, 1078–1088. [CrossRef]

20. Yi, W.J.; Shi, X.D. Numerical simulation analysis for RC shear walls under impact load. *J. Vib. Shock.* **2019**, *38*, 102–110. (In Chinese)

21. Luo, J.; Xiao, J.C.; Ma, K.J.; Mao, J.Y.; Zhang, H. Energy dissipation performance of a sand cushion on steel-concrete composite beam under the impact load of rockfall. *J. Vib. Shock.* **2019**, *38*, 249–256. (In Chinese)

22. Broadhouse, B.J.; Neilson, A.J. Modelling reinforced concrete structures in DYNA-3D. In Proceedings of the DYNA3D User Group Conference, London, UK, 24 September 1987.

23. Broadhouse, B.J. *The Winfrith Concrete Model in LS-DYNA3D*; Rep. SPD/D(95)363; Structural Performance Department, AEA Technology, Winfrith Technology Centre: Carlsbad, CA, USA, 1995.

24. Hallquist, J.Q. *LS-DYNA Keyword User's Manual, Revision 971*; Livermore Software Technology Corporation: Livermore, CA, USA, 2007.

25. Zhu, X.Y.; Pan, R.; Lin, G.; Li, L. FEM analysis of impact experiments with steel plated concrete walls based on ANSYS/LS-DYNA. *Explos. Shock. Waves* **2015**, *35*, 222–228. (In Chinese)